

Assessment of grass lodging using texture and canopy height distribution features derived from UAV visual-band images

Suiyan Tan ^{a,b}, Anders Krogh Mortensen ^b, Xu Ma ^c, Birte Boelt ^b, René Gislum ^{b,*}

^a College of Electronic Engineering, South China Agricultural University, Guangzhou, China

^b Department of Agroecology, Aarhus University, Slagelse, Denmark

^c College of Engineering, South China Agricultural University, Guangzhou, China



ARTICLE INFO

Keywords:

Lodging severity
Unoccupied aerial vehicle
Support vector machine
Histogram of oriented gradients
Canopy height distribution

ABSTRACT

Lodging is a major limiting factor for the yield, quality and harvesting efficiency of selected crops worldwide. This study presents an efficient, robust and non-destructive assessment of lodging severity for four different grasses for seed production, using images collected by an unoccupied aerial vehicle (UAV) in two field plot experiments across five growing seasons. Canopy texture and height related features were extracted from individual plot images and evaluated for estimating lodging severity. Histograms of oriented gradients (HOG) were used as texture features, and three canopy height distributions features (CHV1, CHV2 and CHV3) were proposed. Each canopy height distribution feature divides the plots into subplots and estimates the average height of each subplot. CHV1 concatenates average height of the subplots into its feature, while CHV2 concatenates the difference in average height between all subplots, and CHV3 concatenates the difference in average height between adjacent subplots. The plots were classified using support vector machines into three categories according to the lodging severity. The results showed that the HOG and height distribution features can be used for grading lodging severity in UAV images with high accuracy (71.9% and 79.1%, respectively). However, the HOG features showed a negative relationship to the ground sample distance (GSD), while the CHV1 had a constant accuracy across the GSDs. Combination of the two features did not significantly improve the classification accuracy. The present results have potential to generate lodging severity maps for application in precision farming and thereby to increase grass seed yield and harvest efficiency at farm scale. It should be noted that results and methods from the current study might not be transferred to other crops due to crop specific lodging characteristics and effect of yields.

1. Introduction

Grass is used extensively in temperate pastures as a high-quality source for feeding animals or as turf for home lawns, golf courses and recreational areas (Abel et al., 2017). Grassland is estimated to cover approximately 72 million hectares within the European Union with grass seed production estimated at a total value of 23 billion Euro (ESA, 2016). Seed yield is a key trait for all forage and turf grass species (Boelt and Studer, 2010). Lodging, which is the permanent displacement of a crop stalk from its natural upright position and is due to internal and external factors, is a major limiting factor for the yield, quality and harvesting efficiency of crops worldwide (Berry and Spink, 2012; Griffith, 2000; Kendall et al., 2017; Niu et al., 2012).

Several studies have been performed to analyse the mechanism and

the cause of crop lodging (Brune et al., 2018; Xue et al., 2017; Baker et al., 1998), which have presented quantitative measures to evaluate lodging resistance of individual crops. However, it is often of interest to assess the severity of lodging and to map the seasonal lodging risk in an entire crop field; thus, monitoring and assessing lodging severity occupy an important role in the research of crop lodging. The traditional method to identify the lodging area and lodging severity relies on manual field assessments, which are labour intensive, time consuming and subjective. When large and entire fields are involved, manual inspection is infeasible. Thus, one possible solution is to use image analysis to give an objective assessment of the field and to use remote sensing technique to capture the images in order to reduce the overall labour and time.

* Corresponding author.

E-mail address: rg@agro.au.dk (R. Gislum).

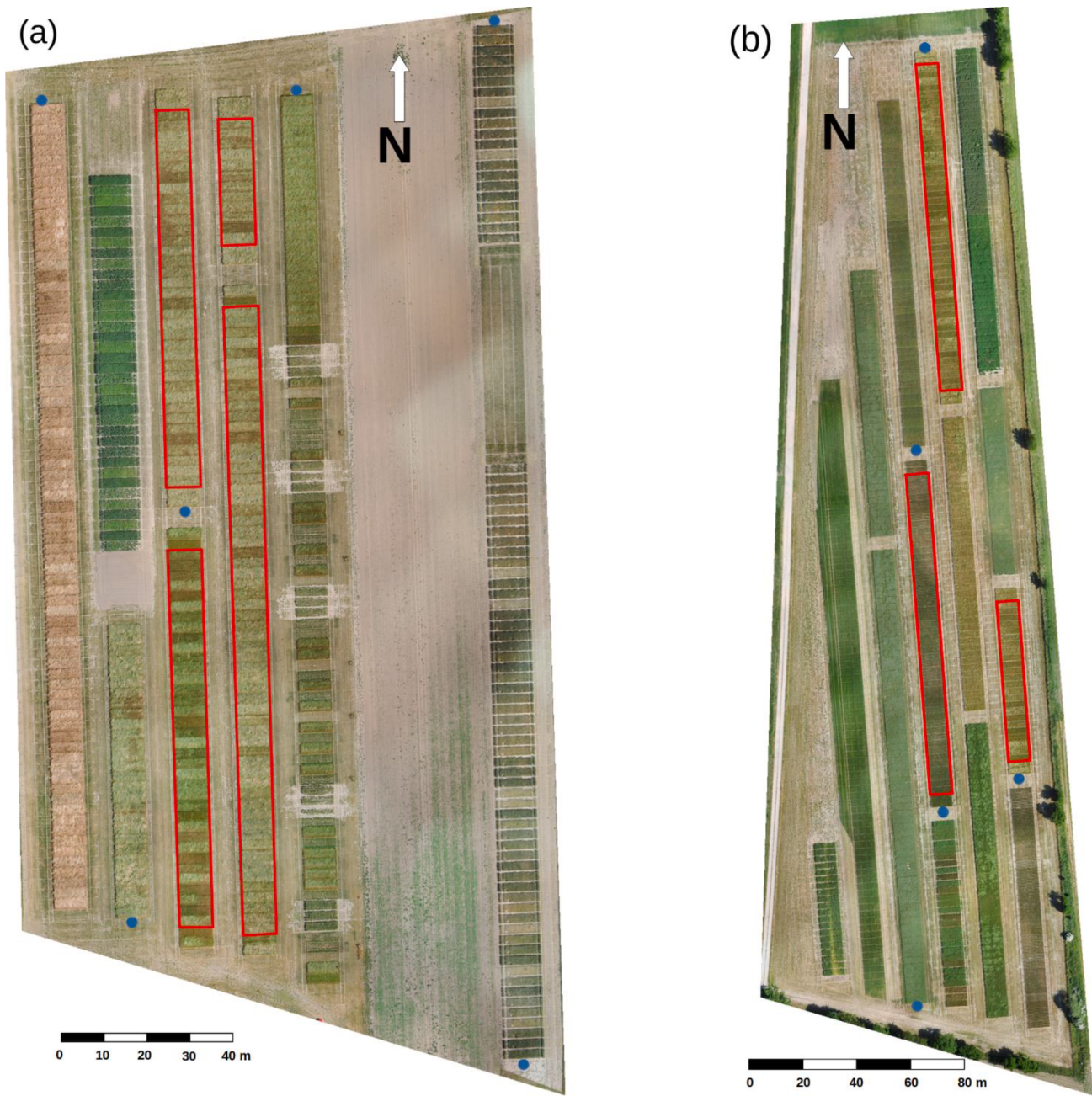


Fig. 1. Overview of the two locations (a) Mindelundsvej and (b) Bjaerup from 2018. The plots highlighted in red were the plots included in this experiment. The blue circles show the locations of the ground control points.

1.1. Related work

Static digital images obtained from ground-based devices have been used to assess crop lodging. Ogden et al. (2002) proposed a functional regression assessment metric to predict the lodging severity based on images acquired at a 3-metre height nadir-view over a rice field. Masuda et al. (2013) used variances of pixel values in the subbands acquired by wavelet transform as features to judge whether rice plant lodging occurred or not by a threshold method. Zhang et al. (2012) detected grain quality of maize plant under lodging and non-lodging circumstances, using a ground-based spectrometer. In their study, distinguishable spectral features were extracted by utilising the continuous wavelet transform method and the partial least squares regression. To extend usability of these methods at large farm scale, calibration and re-evaluation are required.

Large areas can quickly and easily be scanned using different sensor technologies because of the rapid development of remote sensing. Combined with image analysis, this technology may provide efficient and reliable tools for obtaining timely grass lodging information over a large area of the field. Sensors can acquire data remotely while being on board different platforms, such as satellites, airplanes and unoccupied aerial vehicles (UAVs) (Kasampalis et al., 2018). Radar-based satellite data have also been reported as a method to detect lodging. Yang et al. (2015) investigated using RADARSAT-2 radar satellite imagery and found that polarimetric features, such as the backscattering intensities and scattering components from polarimetric decompositions, were sensitive to the lodging of wheat. However, their study did not provide quantitative information on lodging monitoring. Chen et al. (2016) found similar results in sugarcane lodging detection. Han et al. (2018a) found a correlation between a Sentinel-1 radar polarisation index and

corn height and used it to detect corn lodging. Unfortunately, back-scatter and polarimetric features are also related to crop growth, senescence and density; hence, these methods can only be applied at certain growth stages.

Compared to satellite and airplane, a UAV with proper sensors offers a flexible, convenient and cost-effective way to provide desired and high-resolution images of crop fields. Previous work on lodging assessment using UAVs have studied colour, texture and height derived from RGB images as well as temperature. Rajapaksa et al. (2018) used grey-level co-occurrence matrix texture features and support vector machine (SVM) to show the presence and absence of lodging in wheat and canola at a subplot scale. Yang et al. (2017) constructed a pixel-wise classifier to classify rice as lodging or non-lodging using RGB colour, texture and digital surface model (DSM) extracted from UAV images. Han et al. (2018b) proposed a method using similar features and two nomogram models to predict the probability of maize lodging and to identify the protective factors and risk factors related to maize lodging. However, the stability of the predicted model needed further study due to lack of data validation for multiple growing stages. Chu et al. (2017) used the UAV-estimated maize height to assess maize lodging severity. This proposed method segmented the individual maize rows into multiple grid cells and determined the lodging severity on a per-plant basis based on the height percentiles against pre-set thresholds within individual grid cells. However, threshold tuning was inevitably required for adapting this method to a variety of plant types over different growth stages. Similarly, canopy height measurement by small-balloon photogrammetry was employed to evaluate lodging rate in a buckwheat area (Murakami et al., 2012). More recently, Liu et al. (2018) found that temperature was distinct between lodging and non-lodging rice areas, and an SVM lodging recognition model using colour, texture and temperature indices was established. The temperature indices were collected using a handheld platform while the colour and texture indices were collected using a UAV.

Although much progress in the assessment and prediction of crop lodging has been made, we suggest some areas that can be further improved. The previous studies primarily perform binary classification into lodging or not lodging. In pixel-wise classification, this may lead to the “salt and pepper” effect, where single pixels in a larger area are misclassified (Orynbaiyzy et al., 2019). This effect may be circumvented by grouping pixels before classifying them jointly. When classifying groups of pixels, the classification problem is, however, no longer necessarily binary, since some pixels may correspond to lodging and others not. A second area is utilisation of a standard lodging scale. Currently there are no standard reference scale to represent lodging in a more detailed way (e.g. mild, moderate and severe), and we suggest a lodging scale that can be utilised worldwide in different crops.

To overcome these limitations, features that are different from previous studies should be explored and adopted. Features used alone or combined should be sensitive to different lodging severity. Furthermore, a method to measure and to validate different lodging severity of small areas, such as individual plots, should be adopted to avoid the shortcoming of pixel-wise classification. In extension to this, a non-binary lodging classification should be developed (e.g., mild, moderate and severe lodging). In the event of lodging, the crop canopy structure is destroyed so that the stem is inclined at a certain angle and the plant height is reduced. As a result, both texture and the crop height distribution within the canopy change. Histograms of oriented gradient (HOG) is a feature representing an image with a set of local histograms counting the occurrences of gradient orientations within a local image cell. It was successfully applied for pedestrian detection by Dalal and Triggs (2005), and it was found that the HOG features significantly outperformed existing feature sets for human detection. Meanwhile, crop height has been widely used in establishing the crop yield models that translate the relationship between crops and their environment (Borra-Serrano et al., 2019; Caruso et al., 2019; Hassan et al., 2019). To our best knowledge, HOG features and crop height distribution have not

Table 1

Overview of manual lodging scoring dates, location, days from scoring to UAV flight and number of plots with given lodging severity. Min and Bj correspond to Mindelundsvej and Bjaerup field locations, respectively. No, medium and severe lodging correspond to lodging scores of 0-30, 31-60 and 61-100, respectively.

Scoring date (yyyy.mm.dd)	Field	Days till flight	Number of plots		
			No lodging	Medium lodging	Severe lodging
2016.06.08	Min	-1	23	28	5
2017.07.05	Bj	+2	0	26	22
2017.07.05	Min	+2	39	19	30
2018.05.14	Min	0	192	0	0
2018.05.23	Min	0	190	2	0
2018.05.29	Min	0	153	38	1
2018.06.08	Bj	0	120	0	0
2018.06.12	Min	0	61	57	110
2018.06.26	Min	-1	42	37	149
2019.05.10	Min	-2	116	0	0
2019.05.15	Bj	-1	112	0	0
2019.05.29	Min	-1	102	6	0
2019.06.04	Min	0	74	89	1
2019.06.05	Bj	-1	111	1	0
2019.06.21	Min	-1	0	42	66
2019.06.21	Bj	0	93	18	1
2019.06.27	Min	+1	0	8	52
2020.05.28	Min	0	283	5	0
2020.06.03	Min	0	301	67	0
2020.06.04	Bj	-1	248	0	0
2020.06.12	Bj	0	248	0	0
2020.06.12	Min	0	182	182	4

previously been studied for crop lodging severity assessment.

The objective of this study is to explore an efficient and robust way to assess the lodging severity using four different grass seed crops as model crops. For this purpose, an RGB camera mounted on a UAV is used to capture images of a field plot experiment. Two types of features extracted from the individual plots are investigated: (i) HOG feature and (ii) canopy height distribution. An SVM classifier is used to classify the individual plots into three lodging categories: no lodging, medium lodging and severe lodging.

2. Materials and methods

2.1. Field experiments

The present study was part of two comprehensive field plot experiments conducted at two locations at Research Centre Flakkebjerg, Denmark ($55^{\circ}32' N$ and $11^{\circ}39' E$), from 2016 to 2020. The two locations were Bjaerup (Bj) and Mindelundsvej (Min) (Fig. 1). The size of each plot was $2.5 \times 8 m^2$. The soil at Flakkebjerg is classified as a sandy loam (Haplic Luvisol (FAO)/Typic Hapludalf (USDA)) with clay illuviation below the plough layer (23 cm) and sand lenses. The experimental design was a fully randomised design with four replicates. Red fescue (*Festuca rubra* L.), Perennial ryegrass (*Lolium perenne* L.), Tall fescue (*Festuca arundinacea* L.) and Cocksfoot (*Dactylis glomerata* L.) was managed according to best agricultural practice, and different strategies for plant growth regulators were applied in each plot from 2016 to 2020. Each plot was manually given a lodging score from mid-May until mid-July based on the spatial extent of lodging. The lodging scores ranged from 0 to 100 with higher scores corresponding to more severe lodging. If 20% of the plot was lodged, then the individual plot was given a lodging score of 20. After the manual assessment, the lodging scores were grouped into three categories: no lodging for lodging scores of 0-30, medium lodging for lodging scores of 31-60, and severe lodging for lodging scores of 61-100. Manual lodging scores of each individual plot were given on the flight dates or within one or two days of the flight date (Table 1).

Table 2

The technical specification of each flight, including date, field, average flight height, ground sample distance (GSD) and the mean localisation error of the GCPs in the East (E), North (N) and altitude (A). Min and Bj correspond to Mindelundsvej and Bjaerup field locations, respectively.

Flight date (yyyy, mm.dd)	Field	Sensor	GSD (cm/pixel)	GCP error (cm)		
				E	N	A
2016.06.07	Min	Canon	1.40	0.30	0.60	1.70
2017.07.07	Bj	SODA	2.27	0.10	0.13	0.69
2017.07.07	Min	SODA	2.26	0.02	0.06	0.78
2018.05.14	Min	SODA	1.38	0.24	0.14	0.11
2018.05.23	Min	SODA	1.48	0.11	0.07	0.18
2018.05.29	Min	SODA	1.46	0.16	0.35	0.72
2018.06.08	Bj	SODA	1.53	0.01	0.03	0.25
2018.06.12	Min	SODA	1.53	0.44	0.04	0.90
2018.06.26	Min	SODA	1.47	0.50	0.02	0.41
2019.05.08	Min	SODA	1.50	0.14	0.02	0.22
2019.05.14	Bj	SODA	1.50	0.65	1.82	12.85
2019.05.28	Min	SODA	1.50	0.02	0.11	0.09
2019.06.04	Min	SODA	1.49	0.00	0.01	0.00
2019.06.04	Bj	SODA	1.53	0.00	0.07	0.12
2019.06.20	Min	SODA	1.47	0.00	0.00	0.01
2019.06.21	Bj	SODA	1.51	0.01	0.01	0.02
2019.06.28	Min	SODA	1.49	0.00	0.00	0.00
2020.05.28	Min	SODA	1.50	0.57	0.33	1.22
2020.06.03	Min	SODA	1.48	0.01	0.01	0.01
2020.06.03	Bj	SODA	1.54	0.04	0.04	0.00
2020.06.12	Bj	SODA	1.51	0.00	0.00	0.03
2020.06.12	Min	SODA	1.52	0.04	0.03	0.05

2.2. Image acquisition

Images were captured nadir with 80% frontal and side overlap (**Table 2**) using either a Canon PowerShot ELPH 110 HS (Canon, Tokyo, Japan) or senseFly S.O.D.A. (senseFly, Cheseaux-Lausanne, Switzerland) mounted on the eBee (senseFly, Cheseaux-Lausanne, Switzerland). Images captured with the Canon camera were captured with a fixed focal length of 4.3 mm, single shot auto focus and a hyperfocal distance of 1.28 m. Images captured by the S.O.D.A. camera had a fixed focal length of 10.6 mm, single shot auto focus and a fixed hyperfocal distance of 3.53 m. See “Appendix A – Camera specifications” for more details. The eBee was launched by hand. While flying, image capturing and landing were performed automatically using eMotion (senseFly, Cheseaux-Lausanne, Switzerland). Ground control points (GCPs) were placed around the plot experiments with fixed positions throughout each growth season (**Fig. 1**).

The images collected from a specific field on a given day were processed into a DSM and orthomosaic (**Fig. 2**) using the photogrammetry software Pix4Dmapper (Pix4D S.A., Prilly, Switzerland). The standard three-step semi-automated processing workflow was used, which includes the “Initial Processing”, “Point Cloud and Mesh” and “DSM, Orthomosaic and Index” steps. Prior to processing the images, the GCPs were detected in the images using the Drone Dataflow toolbox (Mortensen et al., 2019) for MATLAB (version 2018b, the MathWorks, Inc., Natick, Massachusetts, United States). The detected GCP image positions were imported into Pix4D to improve the geographical accuracy of the DSM and orthomosaic. The individual plots were extracted from the DSM and orthomosaic using the Drone Dataflow toolbox based on the global positioning system (GPS) coordinates of the corners of the individual plot. The GPS coordinates of the plot corners and the GCPs were collected using an RTK GPS receiver (GRS-1s, Topcon Positioning Systems Inc., Livermore, CA, USA) in the field.

2.2.1. Plot image preprocessing

The axes of the extracted plots were not aligned with the image axes. Furthermore, the size of the extracted plots measured in pixels varied because of varying GSD. Therefore, the DSM and orthomosaic of the extracted plots were pre-processed to normalise the plots before feature

extraction (**Fig. 2**). The preprocessing was performed using MATLAB in the following three steps. First, the plot image was rotated to align the plot with the image axes. Next, the largest rectangle fitting inside the plot was extracted. Finally, the extracted plot was resized to a 167 × 533 pixels corresponding to a GSD of 1.5 cm/pixel, so that the extracted plots had the same size in pixels.

2.2.2. Dataset

The full dataset consists of 3756 plot images with 2690 plot images with no lodging, 625 with medium lodging and 441 with severe lodging (**Table 1**). To ensure an independent test, all plot images from a single year were selected for the test set. 2019 were selected for the test set, as it showed the most balanced distribution between the three classes, while having a sufficiently large number of samples. The plot images from the remaining years (2016, 2017, 2018 and 2020) formed the basis for the training and validation sets. 80% of these plot images in each lodging severity group were randomly selected for the training set, while the remaining 20% were selected for the validation set. In the training set, the number of plot images in three lodging severity groups were 1665 of no lodging, 368 of medium lodging and 256 of severe lodging, respectively. In the validation set, the number of plot images in three lodging severity groups were 417 of no lodging, 93 of medium lodging and 65 of severe lodging respectively. In the test set, the number of plot images in three lodging severity groups were 608 of no lodging, 164 of medium lodging and 120 of severe lodging respectively.

2.3. Texture feature of individual plot

HOG (Dalal and Triggs, 2005) was used to capture and express textures caused by different lodging severity in the plots. To extract the HOG feature of a plot, the extracted plot image was divided into uniformly spaced non-overlapping cells of $C \times C$ pixels (**Fig. 3**, top). The image gradient orientation of each cell was binned and aggregated into local histograms. Dalal and Triggs (2005) found that using an unsigned gradient orientation (0–180°) and 9 bins performed better than a lower number of bins and a signed gradient orientation (0–360°) with an increased number of bins (up to 18 bins). Therefore, the histogram binning was performed using the unsigned gradient orientation and 9 bins in this work. The cells were grouped into overlapping blocks of $B \times B$ cells. As such, a single cell could be included in multiple blocks. The cell histograms in each block were normalised with respect to the entire block. The HOG feature is thus comprised of all the normalised histograms of the gradient orientations (**Fig. 3**, bottom). The cell size C and block size B were optimised through a grid search during training of the classifier, and the block overlap was fixed to half the block size rounded up to reduce the search space.

2.4. Grass height distribution at plot scale

2.4.1. Grass height extraction

The area outside the plots was mowed weekly to keep the ground flat and neat. Therefore, it was fairly constant in height and could be used as reference height of the plots. For a given plot, a 1-m long strip with the same width as the plot was extracted at each end of the plot (**Fig. 4**). The average height of the two strips was used as the reference height of the plot. The pixel-wise grass height within the plot was then calculated by subtracting the reference height from the DSM (**Fig. 4**).

2.4.2. Grass height distribution

To quantify the canopy height distribution of a plot, the plot was divided into $n \times m$ subplots, where n and m are the number of rows and columns, respectively. In the following, three grass height distribution vectors derived from the subplots are proposed to describe the canopy structure and to assess the lodging severity of the individual plots.

The first grass height distribution vector, CHV1, calculates and concatenates the average height of each subplot. For example, the

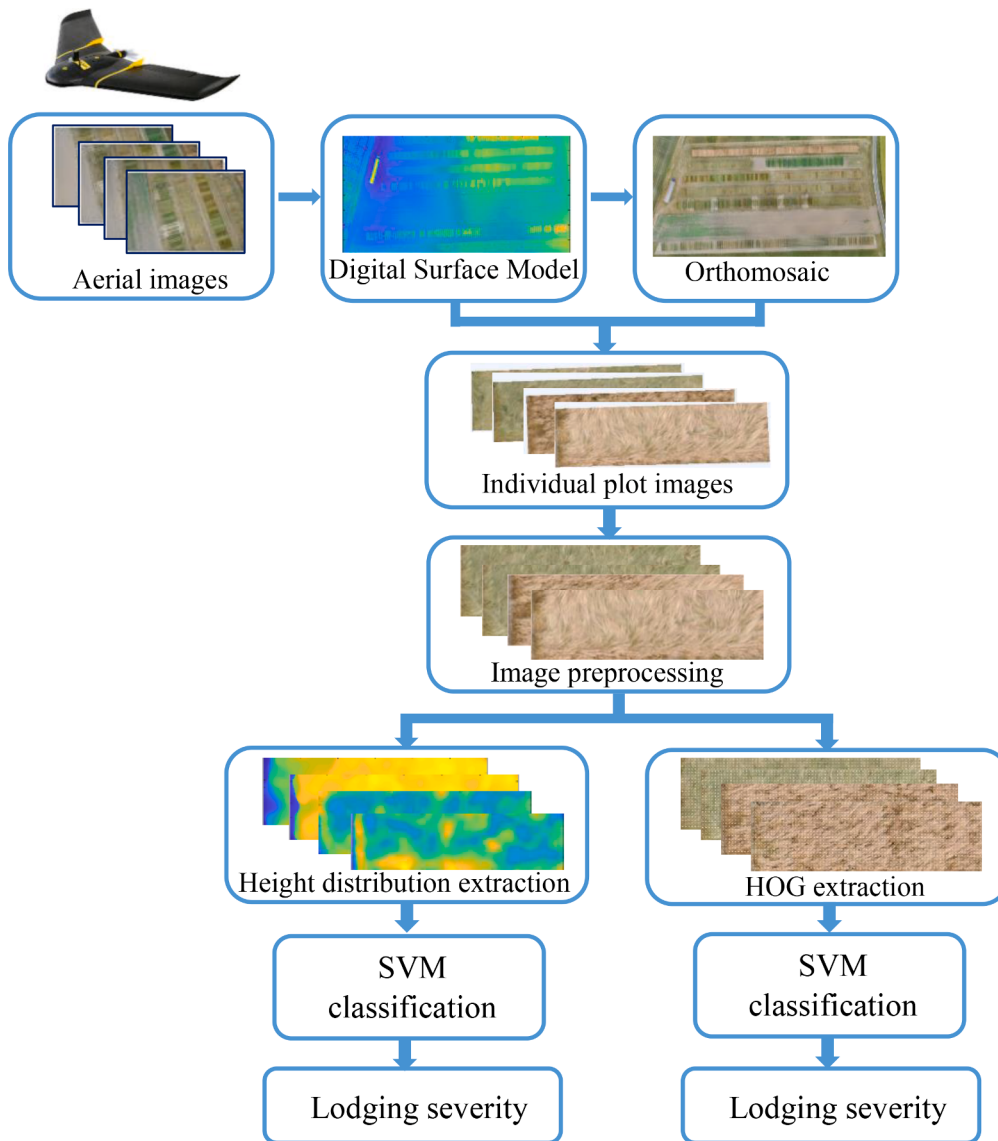


Fig. 2. Flowchart of UAV-based grass lodging severity assessment.

average height of the subplot of the i th row and the j th column is denoted as \bar{h}_{ij} . CHV1 is a vector concatenating the average height of all subplots, which is marked as $CHV1 = [\bar{h}_{1,1}, \bar{h}_{1,2}, \dots, \bar{h}_{ij}, \dots, \bar{h}_{n,m}]$.

The second grass height distribution vector, CHV2, extends CHV1 by also considering the height difference between any two subplots, $\Delta CH_{i,j,p,q} = \bar{h}_{ij} - \bar{h}_{p,q}$. It is clear that $\Delta CH_{i,j,p,q} = -\Delta CH_{p,q,i,j}$. Thus, to avoid redundant calculations, only subplot pairs where $p > i$ and $q > j$ when $p = i$ are included in CHV2.

Similarly to CHV2, the third grass height distribution, CHV3, also extends CHV1 by considering the height difference between subplots. In contrast to CHV2, CHV3 only considers the height between adjacent subplots. To avoid redundant calculations, CHV3 only includes $\Delta CH_{i,j,p,q}$, where $p = i$, $q = j + 1$ or $p = i + 1$, $q = j$.

With varying row numbers n and column numbers m , the plot can be divided into different numbers of subplots; therefore different height distribution vectors are formed. Increasing the number of rows or columns increases the number of subplots, which increases the spatial level of detail of the height distributions. However, this also increases the number of feature dimensions fed to the classifier, which may make it harder to train and generalise.

2.5. Classifier and hyperparameter optimisation

A multiclass SVM was adopted to classify the plots according to their lodging severity based on the HOG and height distribution features (CHV1, CHV2 and CHV3). For each multiclass SVM, a set of three one-versus-one binary SVM classifiers corresponding to the three unique pairs on lodging severities was trained. For each multiclass SVM, the accuracy and the precision and recall of the individual lodging severities were noted. The accuracy, precision and recall are given by:

$$\text{accuracy} = \frac{\#\{\text{correctly classified plots}\}}{\#\{\text{plots}\}}$$

$$\text{precision}(LS) = \frac{\#\{\text{plots with LS classified as LS}\}}{\#\{\text{plots classified as LS}\}}$$

$$\text{recall}(LS) = \frac{\#\{\text{plots with LS classified as LS}\}}{\#\{\text{plots with LS}\}}$$

where LS is the lodging severity 'No', 'Medium' or 'Severe'.

The HOG and height distribution features have two hyperparameters each, which were optimised through a grid search on the training set by training a multiclass SVM for each combination and evaluating it on the

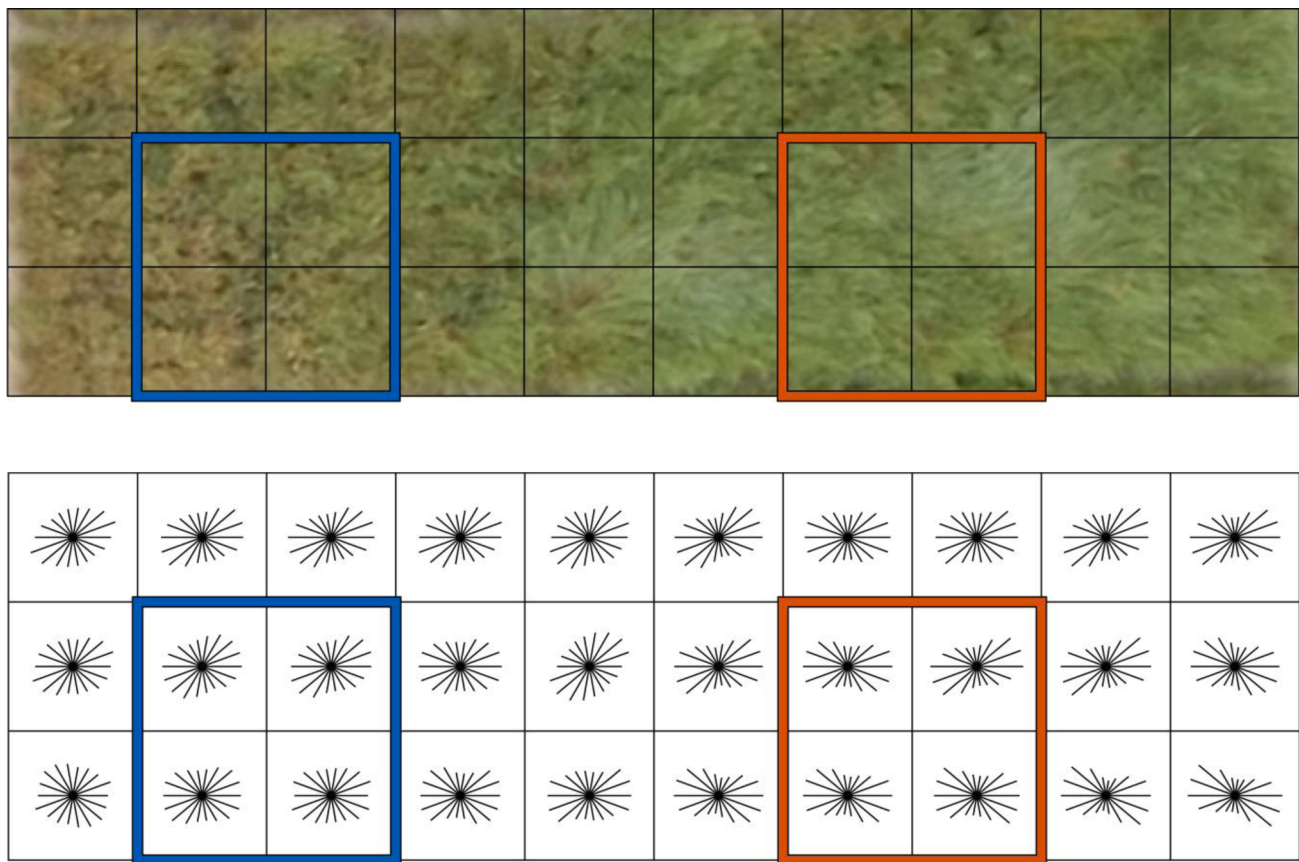


Fig. 3. Example of histogram of oriented gradients (HOG) of a plot using a cell size of 60×60 pixels and a block size of 2×2 cells. Top: plot image divided into cells. Two blocks covering non-lodging and lodging areas are highlighted in blue and red, respectively. Bottom: Visualisation of the extracted HOG feature. The relative length of each line indicates the relative number of gradients with that orientation within that cell.

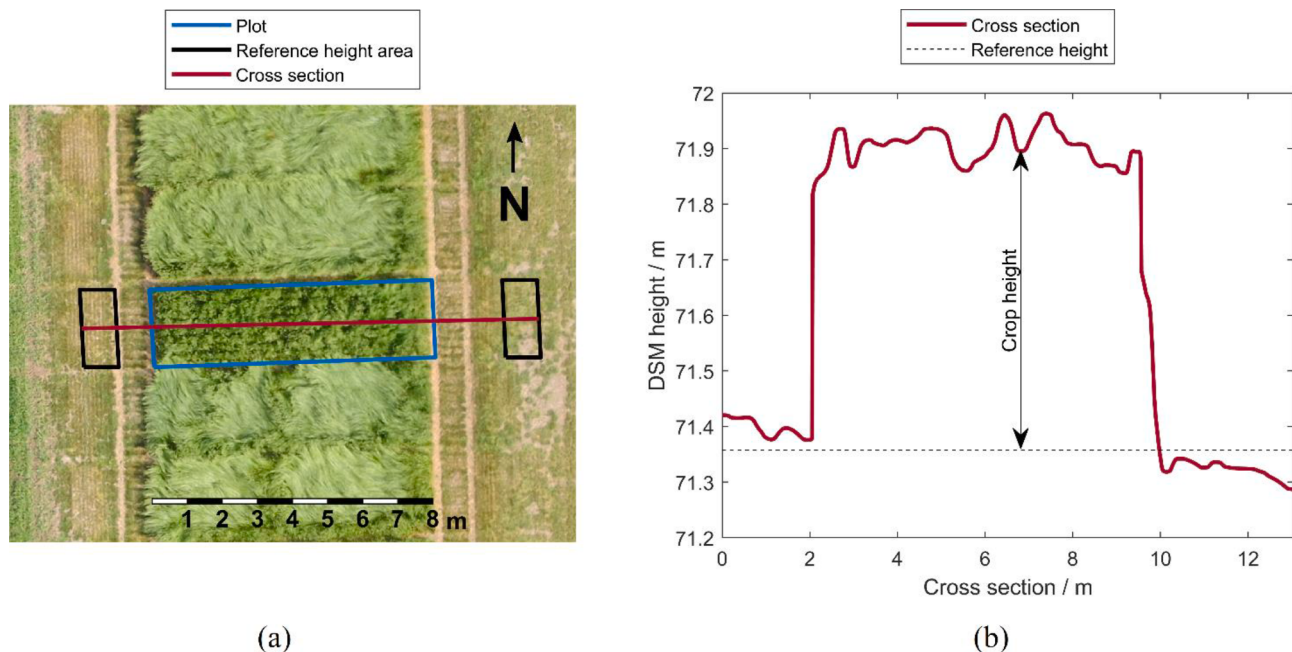


Fig. 4. Grass height extraction from reference height. (a) Overview of plot, areas used for extracting reference height and cross section. (b) Grass height and DSM height along the cross section from (a).

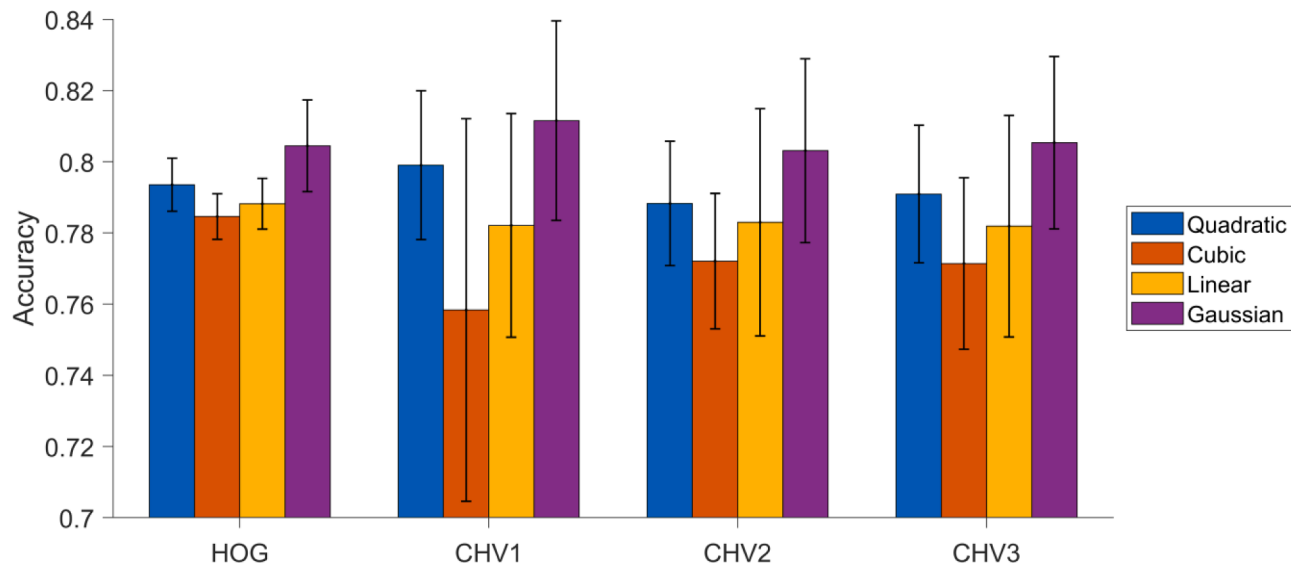


Fig. 5. Bar plot of average accuracy on the validation data across all SVMs trained on the Histogram of Oriented Gradients (HOG) and height distribution features CHV1, CHV2 and CHV3, respectively. For HOG, SVMs trained with cell sizes of 8, 16 and 32 and block sizes of 2-6 were included. For CHV1-3, SVMs trained with 2-6 rows and 4, 6, 8, 10, 15, 20 and 25 columns were included. The bars are grouped by features and kernels (quadratic, cubic, linear and Gaussian). Error bars show the standard deviation across the SVMs.

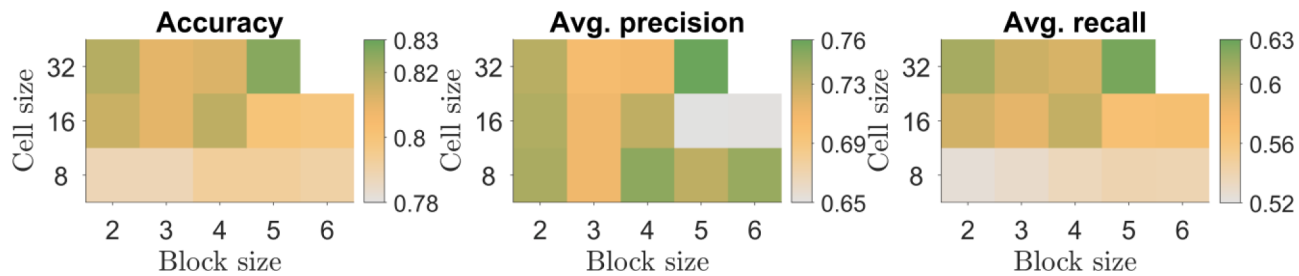


Fig. 6. Results for the Histogram of Oriented Gradients (HOG) parameter grid search on the validation set. (a) Overall accuracy, (b) average precision and (c) average recall of lodging severity classification on the validation set using only the HOG feature.

validation set. For the HOG feature, the hyperparameters were the cell size $C \in \{8, 16, 32\}$ and the block size $B \in \{2, 3, 4, 5, 6\}$. For the height distribution features, the hyperparameters were the number of rows $n \in \{2, 3, 4, 5, 6\}$ and the number of columns $m \in \{4, 6, 8, 10, 15, 20, 25\}$. Linear, Quadratic, Cubic and Medium Gaussian kernels were evaluated as kernel function for each of the SVMs trained in the grid searches. The kernel with the highest average accuracy on the validation set across the grid search of each texture and height feature (HOG, CHV1, CHV2 and CHV3) was selected as kernel function. After selecting the optimal kernel function, the highest accuracy on the validation set was used to select the hyperparameters.

Feature extraction and analysis were performed in MATLAB (version 2018b, the MathWorks, Inc., Natick, Massachusetts, United States) using the Computer Vision System Toolbox 8.2 and the Classification Learner App from the Statistical and Machine Learning Toolbox 11.4.

Table 3

Confusion matrix for SVM using HOG feature with cell size of 32 and block size of 5 evaluated on the test set. The lower right cell shows the accuracy.

		Predicted	No	Medium	Severe	Recall
Observed	No	606	1	1	99.7%	
	Medium	134	19	11	11.6%	
	Severe	51	53	16	13.3%	
Precision	76.6%	26.0%	57.1%	71.9%		

3. Results and analysis

3.1. HOG features

The HOG feature parameter grid search was performed by training individual SVM classifiers on the training set and subsequently evaluating the classifiers on the validation set and test set. Cell sizes of 8, 16 and 32 pixels as well as block sizes of 2, 3, 4, 5 and 6 cells were evaluated. The combination of a cell size of 32 and block size of 6 was not evaluated because the effective size of a single block exceeded the plot image size. For each combination of cell and block size, an SVM classifier was trained using a Linear, a Cubic, a Quadratic and a Gaussian kernel and evaluated on the validation data (Fig. 5). Across all the cell and block size combinations for the HOG feature, using a Gaussian kernel showed the highest accuracy, on average, on the validation data. Therefore, the Gaussian kernel was chosen in the further analysis of the HOG feature.

Using the Gaussian kernel, the accuracy across the different cell and block sizes varied from 78.8% to 82.6% (Fig. 6(a)). The average precision and average recall both showed a greater sensitivity to the cell and block size in terms of larger ranges (from 65.0% to 75.9% and from 52.5% to 62.6%, respectively). The accuracy and average recall both showed increase on average with an increasing cell size, while constant on average with respect to the block size. The average precision showed no clear trends with respect to cell size or block size (Fig. 6). Across cell and block sizes, the accuracy on the validation set generally decreases

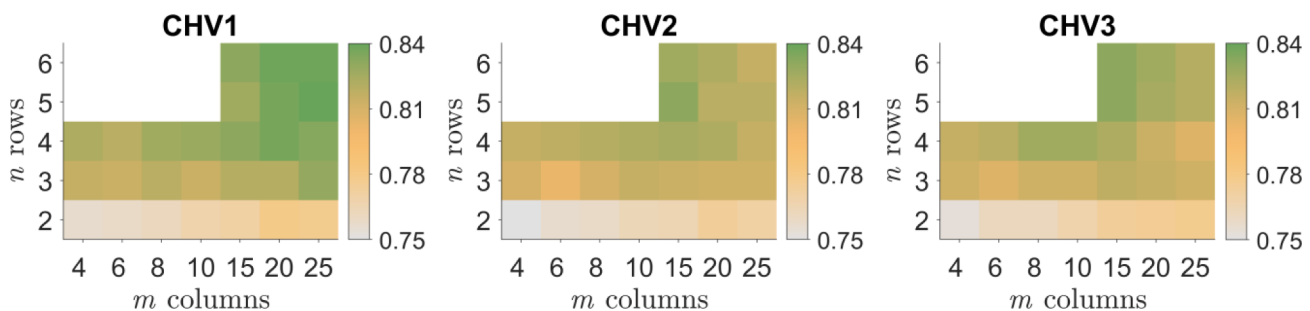


Fig. 7. Overall accuracy on the validation set for the three canopy height distribution vectors (CHV1, CHV2 and CVH3) as a function of the number of subplot rows and columns. The colours indicate the accuracy for a given combination of subplot rows and columns. Combinations with white were not evaluated.

linearly ($R^2 = 0.52$, $p = 0.0023$) with respect to the logarithm of the size of the HOG feature of a single plot image (252 – 22230).

The HOG feature with a cell size of 32 and a block size of 5 resulted in the highest accuracy, average precision and average recall on the validation set, but it was closely followed by a cell size of 32 and block size of 2 and a cell size of 16 and a block size of 4. Therefore, a cell size of 32 and a block size of 5 were chosen as the optimal parameters, which correspond to approximately $0.48 \times 0.48 \text{ m}^2$ and $2.4 \times 2.4 \text{ m}^2$, respectively.

The SVM classifier trained with the HOG feature with a cell size of 32 and a block size of 5 was evaluated on the test set. The ‘No Lodging’ group showed an adequate precision (76.6%) and a high recall (99.7%) (Table 3). The ‘Severe lodging’ group showed an inadequate precision (57.1%) and poor recall (13.3%). The ‘Medium lodging’ group showed poor performance in terms of both precision (26.0%) and recall (11.6%). The poor recall of the ‘Severe lodging’ group on the test set is in contrast to the performance on the validation set, which showed a reasonable recall (67.7%). Similar trends were observed with precision of the ‘Medium lodging’ and ‘Severe lodging’ groups on the validation set (60.6% and 83.0%, respectively) and to a lesser extent for the recall of the ‘Medium lodging’ group (21.5%).

3.2. Canopy height distribution

The three canopy height distribution vectors (CHV1, CHV2 and CHV3) were evaluated at different combinations of subplot rows and columns. The number of rows varied from 2 to 6, while the number of columns varied from 4 to 25. On average, using a Gaussian kernel for the SVM classifier resulted in a higher average accuracy (80.3–81.1%) for all three height distribution vectors on the training data compared to the Quadratic (78.8–79.9%), Cubic (75.8–77.2%) and Linear (78.2–78.3%) kernels (Fig. 5). The difference in average accuracy between the four kernels was larger than for the HOG feature, which shows that the height features were more sensitive to the correct SVM kernel. Therefore, the Gaussian kernels were selected for further analysis of the canopy height distribution vectors.

Using the Gaussian kernel, CHV1 (75.7–84.0%) generally performed better on the validation set than CHV2 (74.6–83.1%) and CHV3 (75.3–83.1%) in terms of accuracy (Fig. 7). On average, the accuracy and average recall of CHV1 increased with the number of rows and columns, while the average precision increased with the number of rows, but varied with the number of columns. Generally, the accuracy increased with the number of subplots the plot images were divided into until the plot image were divided into 125 subplots, where the accuracy peaked. Using two rows, however, provided a significantly lower accuracy compared to the other subplot divisions.

The highest accuracy in CHV1 (84.0%) was found using 5 rows and 25 columns (Fig. 7), and it was therefore selected as the optimal hyperparameters. The accuracy, average precision and recall on the test set were 79.1%, 67.2% and 62.8%, respectively. The ‘No lodging’ and ‘Severe lodging’ groups showed both high precision (78.5–80.3%) and

Table 4

Confusion matrix for SVM using canopy height distribution vector CHV1 with n=5 and m=25 evaluated on the test set. The lower right cell shows the accuracy.

		Predicted			
		No	Medium	Severe	Recall
Observed	No	595	11	2	97.9%
	Medium	129	9	26	5.5%
	Severe	17	1	102	85.0%
Precision	80.3%	42.9%	78.5%	79.1%	

Table 5

Confusion matrix of SVM using combination of HOG (cell size = 32, block size = 5) and height distribution vector CHV1 (n = 5, m = 25). The lower right cell shows the accuracy.

		Predicted			
		No	Medium	Severe	Recall
Observed	No	603	2	3	99.2%
	Medium	139	12	13	7.3%
	Severe	61	15	44	36.7%
Precision	75.1%	41.4%	73.3%	73.9%	

recall (85.0–97.9%), while the ‘Medium lodging’ group showed inadequate precision (42.9%) and poor recall (5.5%) (Table 4).

3.3. Combining texture and canopy height distribution

The HOG feature and height distribution features represent two different indicators of lodging. Combining them may therefore provide a better performance than using them individually. An SVM classifier using both the HOG feature and CHV1 was trained using the optimal settings found in the previous sections. A Gaussian kernel was selected for the SVM classifier since it was the optimal kernel for both HOG and CHV1 (Fig. 5).

Combining the HOG and CHV1 features improved the accuracy, average precision and average recall compared to using only the HOG feature, but it did show improved performance compared to using only the CHV1 feature (Table 5). The improvement compared to using the HOG features mainly stemmed from increased precision of the ‘Medium lodging’ group and increased precision and recall of the ‘Severe lodging’ group. The result indicated that it was hard to improve the accuracy by considering the combination of the HOG feature and height distribution.

3.4. Effect of ground sample distance

The GSD affects the level of details available in the plot images. Increasing the GSD decreases the level of detail, which may obfuscate the differences between the classes. To study the influence of the GSD on the performance of the HOG and CHV1 features, new SVM models were trained on resized plot images. The plot images were resized to sizes

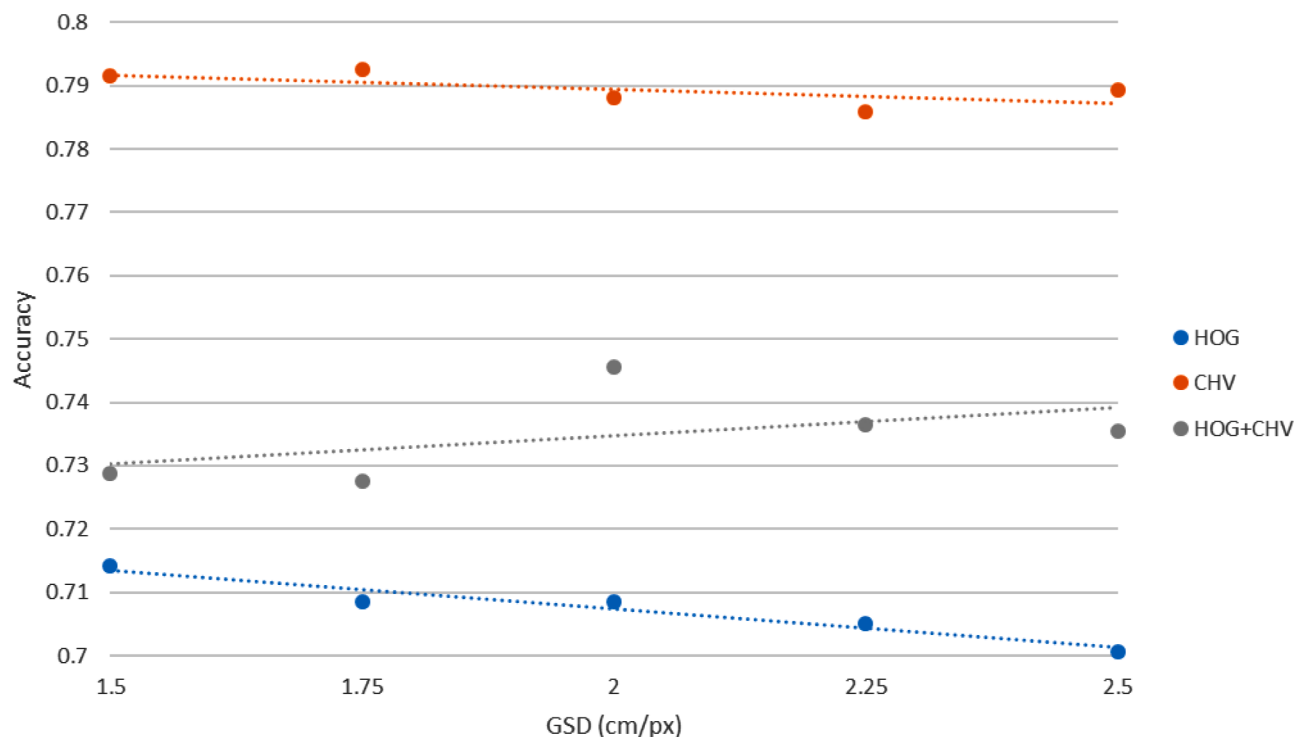


Fig. 8. Accuracy as a function of ground sample distance (GSD) when using the HOG feature, the CHV1 feature and combining them. The plot images were resized to match the desired GSD. The dashed lines show a linear fit to each of three models.

corresponding to GSD of 1.5, 1.75, 2.0, 2.25 and 2.5 cm/px. For HOG, this means that the pixel area covered by a single block using the optimal parameters ($32\text{px per cell} \cdot 5\text{cells per block} = 160\text{px/block}$) is larger than the smallest side of the resized plot images ($167\text{px} \cdot 1.5\text{cm px}^{-1} / 2.5\text{cm px}^{-1} = 100\text{px}$). The HOG model with a cell size of 32 and block size of 2 showed similar results to the optimal parameters on the validation set, hence it was used instead for this GSD study. For CHV1, the previously found optimal parameters were used. The accuracy of the models using the HOG feature showed a negative relationship to the GSD (Fig. 8), that was significantly different from a constant accuracy ($p = 0.007$). The decrease in accuracy for the HOG features is primarily caused by fewer samples being classified as ‘Medium lodging’. The accuracy of the models using the CHV1 feature showed a slight negative relationship to the GSD; however, it was not significantly different from a constant model ($p = 0.22$). The models combining the HOG and CHV1 features showed a positive relationship between the accuracy and the GSD, but it was not significantly different from a constant model ($p = 0.4$).

4. Discussion

4.1. Accuracy of UAV images for grass lodging severity assessment

Based on the existing studies, we find that lodging has been studied most extensively in wheat, followed by barley, rice and cereals in general. In regard to the use of remote sensing to detect lodging, the study is still in an early stage (Chauhan et al., 2019). In previous studies, colour, texture, temperature, spectral and crop height information have been explored as feature parameters to detect crop lodging (Liu et al., 2018; Rajapaksa et al., 2018; Wang et al., 2018; Wilke et al., 2019). In the present study, the test results showed that the HOG feature and height distribution CHV1 achieved accuracy of 71.9% and 79.1%, respectively. Furthermore, when using only CHV1, the high precision and recall in no lodging and severe lodging are comparable with the existing studies (Wang et al., 2018; Wilke et al., 2019; Han et al., 2018a). This demonstrates that CHV1 have strong discriminating abilities in no lodging and

severe lodging in grass seed crops, while the medium lodging needs further investigation.

The height distribution vectors performed well on no lodging and severe lodging but showed significant poorer performance on medium lodging. To test the consistency of classifier over the whole grass growth season, most of the grass phenotyping developments were included in dataset collection. Plot experiments were fully randomly designed with four replicates and applied to different plant growth regulation strategies. Grass height traits exhibited great differences according to growth stage, plant density, cultivars and varieties. Compared with no lodging and severe lodging, medium lodging exhibited variation in height distribution, thus resulting in lower precision.

The low accuracy on the test set from the HOG feature is likely a dimensionality problem. As the feature space becomes too large, the observed data therein becomes too sparse to train generalised classifier. Furthermore, feature vectors representing the same class (e.g., medium lodging) may be located far away from each other in the feature space due to different regions in the plots experiencing lodging (e.g., in either end of the plots). This is also the case for CHV1, but due to a much lower dimensionality of the CHV1 feature, it poses less of a problem there. This is evident by the much higher feature space of the HOG feature (252 – 22230 dimensions) compared to the CHV1 feature (8 – 150 dimensions) and the negative relationship between the accuracy of the HOG feature and the size of the HOG feature space. The HOG feature may further be affected by the environment factors, for example the colour of the grass, illumination and shade. This is particularly evident in medium lodging, which occurs mostly at the middle-late growth stages when the colour of the grass seed crops begins to change from green to yellow. This colour variation unrelated to lodging may result in a change in image gradient, which in turn is encoded in the HOG feature. Furthermore, the high density of the grass canopy causes lodging plants to lay weight on neighbouring plants. Therefore, the neighbour plants exhibit a crop angle of inclination though they are not lodged (Chauhan et al., 2019). This may also cause a gradient change in the images and increase the difficulties in classifying medium lodging.

The HOG and the CHV1 features represent different features of the

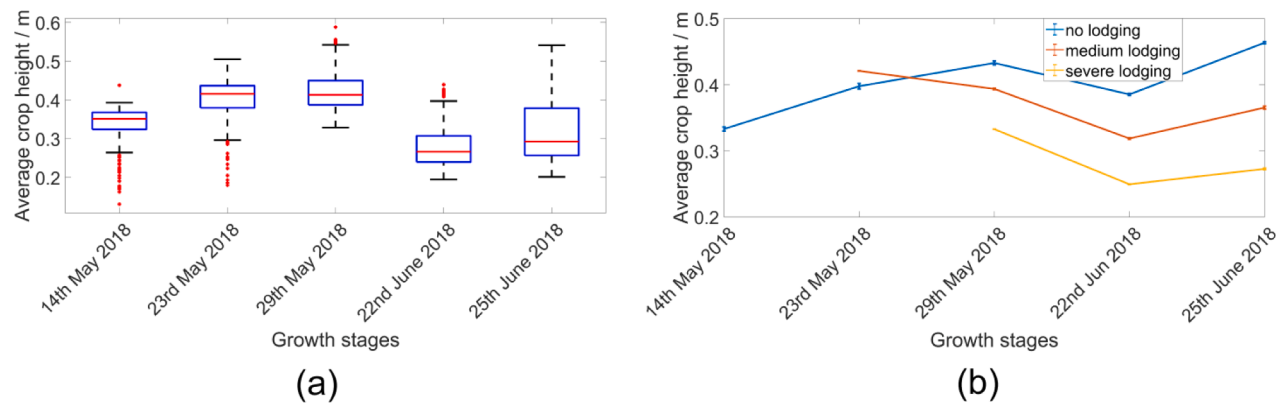


Fig. 9. Average height at plot scale at Min location across the growth stages in 2018: (a) boxplots of the average height (the red central mark on each box represents the median, and the bottom and top edges of the box represent the 25th and 75th percentiles, respectively); (b) average height in different lodging groups.

plots, i.e. the texture and height distribution of the plot, respectively. It was, therefore, expected that combining them would improve the accuracy of the model, however, the combined model only showed an improvement compared to the HOG only models and not the CHV1 only models (Fig. 8). This is likely also a dimensionality problem. Although the CHV1 feature creates a subspace in the combined feature space, which ought to provide the same accuracy as using only the CHV1 features, the addition of the HOG features caused the data to become too sparse to fully utilize the discriminative ability of the CHV1 subspace. In recent years, data-driven approaches commonly known as Deep Learning have become increasingly popular and have shown impressive results within the agriculture domain, e.g. mixed species segmentation (Skovsen et al., 2021) and field crop type classification (Teimouri et al., 2019). Instead of using hand-crafted features such as the HOG feature and the height distribution vectors, a Deep Learning model learns and extracts the features used for the classification task directly from the raw input data. However, Deep Learning models have two major drawbacks compared to traditional methods based on hand-crafted features: 1) large data requirements and 2) computationally expensive. The former can be mitigated through transfer-learning or the use of synthetic data (Skovsen et al., 2017). In an offline system, such as the proposed method, the computational cost is less of a drawback, and it can be

partly mitigated through the selected network architecture, e.g. MobileNet (Howard et al., 2019) or EfficientNet (Tan and Le, 2019). As such, future work exploring Deep Learning models should focus on the data basis, either through acquiring more plots, by utilization other data with transfer learning, or through the use of synthetic data. Future work may also focus on reformulating the task to e.g. binary classification of subplots as either lodging or non-lodging, though this is not specific to Deep Learning.

GSD, as a function of flight height and image resolution, is an important flight parameter. Liu et al. (2018) found that texture features changed significantly, when the altitude of the UAV changed. This supports the decrease in accuracy with increasing GSD for the HOG feature (Fig. 8). However, Mardanisamani et al. (2019) recently proposed a deep convolutional neural network using texture features to classify small plot images into no lodged and lodged areas and the results were promising. In their study, the GSD of images varied from 1.5 to 2.6 cm/pixel, which was similar with the GSD used in our method. Previous studies have demonstrated, that UAV-based crop height can be highly correlated with the ground truth measurements at GSD from 0.45 to 4.0 cm/px (Ampatzidis et al., 2020; Bendig et al., 2014; Borra-Serrano et al., 2020; Chu et al., 2017; Hu et al., 2018; Kawamura et al., 2020; Mai-maitjiang et al., 2020; Poley and McDermid, 2020). This supports the

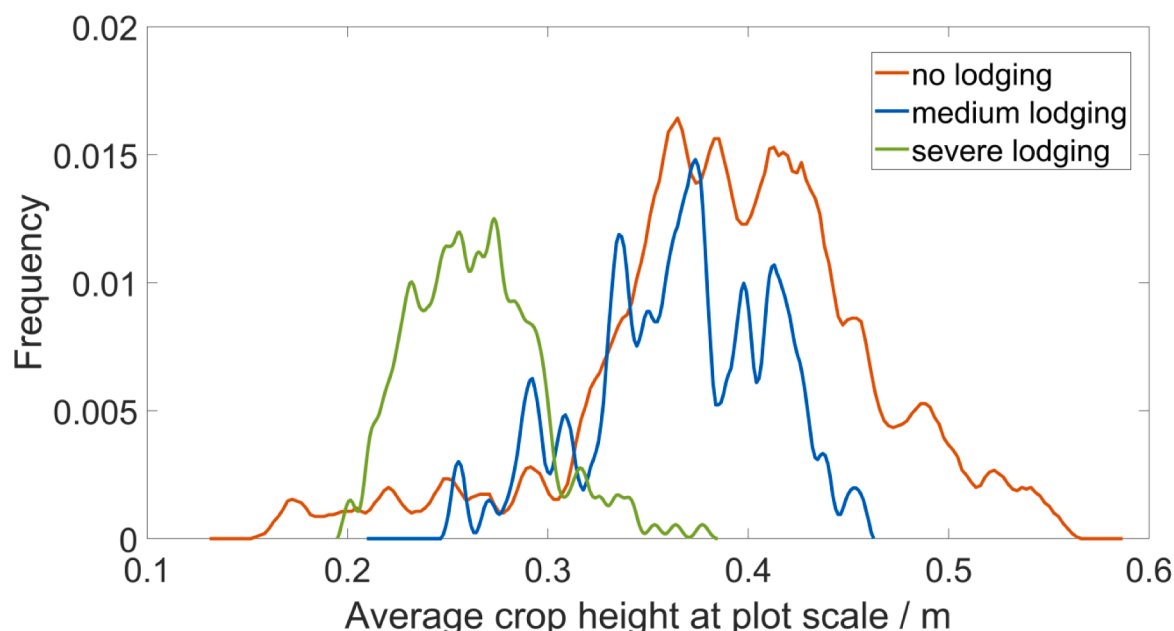


Fig. 10. The frequency of the average grass height in different lodging groups (the curves have been smoothed).

constant accuracy of the CHV1 features across GSDs from 1.5 to 2.5 cm/px (Fig. 8). Therefore, future work using the HOG feature should aim for the lowest possible GSD and flight height, while future work using the CHV1 feature may chose a higher GSD and flight height to cover a larger area.

4.2. Grass seed crops lodging severity comparison over the growth stages

In previous studies, quantitative information for crop lodging monitoring was mainly investigated at certain growth stages (Chen et al., 2016; Han et al., 2018b; Mardanisamani et al., 2019; Yang et al., 2015). To test the consistency of the classification model over the whole growing season and the robustness of our method, image datasets were collected not only across a growth season in 2018 at Min field but were also collected by some individual flight campaigns at two field locations in 2017 and 2016. Canopy structural anomalies were strongly affected by the lodging severity. To examine different lodging severity during a growth season, the average height at plot scale in Min field across the 2018 growth season was presented (Fig. 9). In the early growing season, there is no grass lodging and the average grass height of the plots increased gradually. Medium lodging slows down the grass height growth and will usually start before flowering, which is equivalent to growth stage 57 to 59 at the Biologische Bundesanstalt, Bundesortnamt und Chemische Industrie (BBCH) scale. Attributed to a strong wind according to the weather report, a severe lodging was observed in mid-late June (e.g., 2018.06.22), which corresponded well with a remarkable average height drop. In the following days, weather turned fine, and some part of the grass recovered and straightened up before the flight on 2018.06.25. Therefore, the average height rose a little compared to the flight on 2018.06.22. However, when compared with the early growth stage, most of the lodged grass at harvest stage (i.e. 2018.06.25) was unlikely to straighten up at this later growth stage, presumably, due to taller stems and an increasing weight of the inflorescence, resulting in a low average height. There were wide ranges from the 25th to the 75th percentiles on each box of the flight date (Fig. 9(a)), indicating that the average height of plots exhibits great difference at the same growth stage. The average height in different lodging groups (Fig. 9(b)) was, however, still separated (Fig. 9(b)).

Thus far, we found only one study that classified crop growing area into three lodging severities. Han et al. (2018a) used radar images to classify maize plant area into three lodging severities, and they achieved higher classification accuracy in medium lodging than mild lodging and serious lodging. However, we obtained contrary results, which is probably due to the very different crop architecture between maize and grass and especially the pronounced height difference in lodged and non-lodged maize. Fig. 9 shows that the average grass height of severe lodging is lower than that of no and medium lodging, which demonstrates that severe lodging has a more distinct height distribution. Furthermore, the medium lodging and no lodging groups have similar average height probability with a heavily overlapping area (Fig. 10). It is indicated that the no lodging and the medium lodging groups have great similarity in average grass height at plot scale across the growth stages. This phenomenon probably causes the difficulty in distinguishing medium lodging from no lodging.

4.3. Future application of UAV images in grass seed crops lodging severity prediction for seed production at farm scale

Crop growth is a complex process where weather plays an important role during the spring growing season that affects lodging severity at the later growth stages. Heavy rain, when accompanied by strong winds, can accelerate the lodging process or significantly increase the lodging risk. A daily and long-term routine is of great importance for detection of possible crop lodging. The UAV-based approach facilitates timely, cost-effective and high-throughput capture of crop trait data, making it more suitable for the lodging severity assessment task at medium and large

farm scale compared with the satellite-based remote sensing data. Additionally, only an RGB camera is needed in the proposed method. HOG features can be directly extracted from the RGB images, and grass height distribution can be obtained by using a DTM for the reference height. The DTM can be obtained once before the sowing season and saved for the use of the growth season. In these ways, the time for data collection and processing to detect the lodging severity can be reduced compared to the previous studies that used a combination of different features.

Thus far, because of the absence of a standard reference scale to represent lodging (e.g., mild, moderate and severe), most of previous studies only detected the presence and absence of crop lodging pixel by pixel and calculated the ratio of the lodging area. There is still a lack of the most appropriate method for producing and validating lodging severity and risk maps. To fill the research gap, we proposed a method to measure and validate different lodging severities of small areas such as individual plots in grasses. In comparison, to assess lodging severity directly at local, regional or farm scale, it is more accurate and reliable to operate on individual plots; therefore our method at a certain resolution will be able to show fields or part of the fields where we can expect high risk of lodging and to show which cultivars or areas have an especially high risk of lodging. With the configuration of SVM for lodging severity assessment, it can be further used in precision farming to generate lodging severity maps and to increase grass seed yield and harvest efficiency at farm scale.

5. Conclusion

In this paper, an efficient and robust method of assessing grass seed crops lodging severity using UAV images was presented. Two distinct features, the HOG and canopy height distribution, were derived from individual plot images. SVM classifiers based on the HOG feature and grass height distribution, both combined and individually, were used to classify the individual plots into three lodging severities, namely no lodging, medium lodging and severe lodging. Different parameters of HOG features and three height distribution vectors (CHV1, CHV2, CHV3) parameterised by different numbers of divided subplots were used for SVM classification, and then classification performance was evaluated. The results showed that HOG and height distribution used alone both had satisfactory classification performance for no and severe lodging, while medium lodging requires further investigation. Further, the combination of the two features did not significantly improve the accuracy but showed an improvement in average precision. The study has potential for application in precision farming to generate lodging severity maps and thereby to increase grass seed yield and harvest efficiency at farm scale. It should be noted that grass was used as the model crop in the current study and comparison of results and conclusions to other crops with different lodging characteristics and effect on yield should be avoided. We continue to develop our models to include more years and make the model more robust.

Declaration of Competing Interest

None.

Acknowledgements

We are grateful to the Key-Area Research and Development Program of GuangDong Province under Grants 2019B020214002 and the China Scholarship Council (CSC) for financial support of S.Y. TAN in this work.

Appendix A. Camera specifications

The camera specifications for the two cameras use during images acquisition are listed in Table 6.

Table 6

Camera specifications used during image acquisition.

	Canon PowerShot ELPH 110 HS	senseFly S.O.D.A.
Sensor	Back-illuminated CMOS	Back-illuminated CMOS
Sensor size	1/1.7 inches (7.6×5.7 mm 2)	1 inch (13.2×8.8 mm 2)
Resolution	4608 \times 3456 pixels	5472 \times 3648 pixels
File format	JPEG	JPEG
Focal length (35 mm equivalent)	4.3 mm (24.1 mm)	10.6 mm (28 mm)
Focusing mode	Single shot	Single shot
Hyperfocal distance	1.28 m	1.98–3.53 m
Exposure time	1/1250–1/500 s	1/1000 s
Aperture	f/2.7	f/2.8–f/5.0
ISO	100–125	125–500

References

- Abel, S., Gislum, R., Boelt, B., 2017. Path and correlation analysis of perennial ryegrass (*Lolium perenne* L.) seed yield components. *J. Agron. Crop Sci.* 203 <https://doi.org/10.1111/jac.12202>.
- Ampatzidis, Y., Partel, V., Costa, L., 2020. Agroview: cloud-based application to process, analyze and visualize UAV-collected data for precision agriculture applications utilizing artificial intelligence. *Comput. Electron. Agric.* 174, 105457 <https://doi.org/10.1016/j.compag.2020.105457>.
- Baker, C.J., Berry, P.M., Spink, J.H., Sylvester-Bradley, R., Griffin, J.M., Scott, R.K., Clare, R.W., 1998. A method for the assessment of the risk of wheat lodging. *J. Theor. Biol.* <https://doi.org/10.1006/jtbi.1998.0778>.
- Bendig, J., Bolten, A., Bennertz, S., Broscheit, J., Eichfuss, S., Bareth, G., 2014. Estimating biomass of barley using crop surface models (CSMs) derived from UAV-based RGB imaging. *Remote Sens.* <https://doi.org/10.3390/rs61110395>.
- Berry, P.M., Spink, J., 2012. Predicting yield losses caused by lodging in wheat. *F. Crop. Res.* <https://doi.org/10.1016/j.fcr.2012.07.019>.
- Boelt, B., Studer, B., 2010. Breeding for grass seed yield. In: Boller, B., Posselt, U.K., Veronesi, F. (Eds.), *Fodder Crops and Amenity Grasses*. Springer New York, New York, NY, pp. 161–174. https://doi.org/10.1007/978-1-4419-0760-8_7.
- Borra-Serrano, I., De Swaeft, T., Muylle, H., Nuyttens, D., Vangeyte, J., Mertens, K., Saeys, W., Somers, B., Roldán-Ruiz, I., Lootens, P., 2019. Canopy height measurements and non-destructive biomass estimation of *Lolium perenne* swards using UAV imagery. *Grass Forage Sci* 74, 356–369. <https://doi.org/10.1111/gfs.12439>.
- Borra-Serrano, I., Swaeft, T., De Quataert, P., Aper, J., Saleem, A., Saeys, W., Somers, B., Roldán-Ruiz, I., Lootens, P., 2020. Closing the phenotyping gap: High resolution UAV time series for soybean growth analysis provides objective data from field trials. *Remote Sens.* 12, 1–19. <https://doi.org/10.3390/rs12101644>.
- Brune, P.F., Baumgarten, A., McKay, S.J., Technow, F., Podlány, J.J., 2018. A biomechanical model for maize root lodging. *Plant Soil.* <https://doi.org/10.1007/s11104-017-3457-9>.
- Caruso, G., Zarco-Tejada, P.J., González-Dugo, V., Moriondo, M., Tozzini, L., Palai, G., Rallo, G., Hornero, A., Primicerio, J., Gucci, R., 2019. High-resolution imagery acquired from an unmanned platform to estimate biophysical and geometrical parameters of olive trees under different irrigation regimes. *PLoS One.* <https://doi.org/10.1371/journal.pone.0210804>.
- Chauhan, S., Darvishzadeh, R., Boschetti, M., Pepe, M., Nelson, A., 2019. Remote sensing-based crop lodging assessment: current status and perspectives. *ISPRS J. Photogramm. Remote Sens.* <https://doi.org/10.1016/j.isprsjprs.2019.03.005>.
- Chen, J., Li, H., Han, Y., 2016. Potential of RADARSAT-2 data on identifying sugarcane lodging caused by typhoon. In: 2016 5th International Conference on Agro-Geoinformatics. Agro-Geoinformatics 2016. <https://doi.org/10.1109/Agro-Geoinformatics.2016.7577665>.
- Chu, T., Starek, M.J., Brewer, M.J., Murray, S.C., Pruter, L.S., 2017. Assessing lodging severity over an experimental maize (*Zea mays* L.) field using UAS images. *Remote Sens.* <https://doi.org/10.3390/rs9090923>.
- Dalal, N., Triggs, B., 2005. Histograms of oriented gradients for human detection. In: Proceedings - 2005 IEEE Computer Society Conference on Computer Vision and Pattern Recognition, CVPR 2005. <https://doi.org/10.1109/CVPR.2005.177>.
- ESA [WWW Document], 2016. URL <http://www.euroseeds.eu> (accessed 12.13.16).
- Griffith, S.M., 2000. Changes in dry matter, carbohydrate and seed yield resulting from lodging in three temperate grass species. *Ann. Bot.* 85, 675–680. <https://doi.org/10.1006/anbo.2000.1125>.
- Han, D., Yang, H., Yang, G., Qiu, C., 2018a. Monitoring model of maize lodging based on Sentinel-1 radar image. *Nongye Gongcheng Xuebao/Transactions Chinese Soc. Agric. Eng.* <https://doi.org/10.11975/j.issn.1002-6819.2018.03.022>.
- Han, L., Yang, G., Feng, H., Zhou, C., Yang, H., Xu, B., Li, Z., Yang, X., 2018b. Quantitative identification of maize lodging-causing feature factors using unmanned aerial vehicle images and a Nomogram Computation. *Remote Sens.* <https://doi.org/10.3390/rs10101528>.
- Hassan, M.A., Yang, M., Fu, L., Rasheed, A., Zheng, B., Xia, X., Xiao, Y., He, Z., 2019. Accuracy assessment of plant height using an unmanned aerial vehicle for quantitative genomic analysis in bread wheat. *Plant Methods.* <https://doi.org/10.1186/s13007-019-0419-7>.
- Howard, A., Wang, W., Chu, G., Chen, L., Chen, B., Tan, M., 2019. Searching for MobileNetV3 accuracy vs MADDs vs model size. *Int. Conf. Comput. Vis.* 1314–1324.
- Hu, P., Chapman, S.C., Wang, X., Potgieter, A., Duan, T., Jordan, D., Guo, Y., Zheng, B., 2018. Estimation of plant height using a high throughput phenotyping platform based on unmanned aerial vehicle and self-calibration: example for sorghum breeding. *Eur. J. Agron.* <https://doi.org/10.1016/j.eja.2018.02.004>.
- Kasampalis, D.A., Alexandridis, T.K., Deva, C., Challinor, A., Moshou, D., Zalidis, G., 2018. Contribution of remote sensing on crop models: a review. *J. Imaging* 4. <https://doi.org/10.3390/jimaging4040052>.
- Kawamura, K., Asai, H., Yasuda, T., Khamthavong, P., Soisouvanh, P., Phongchanmixay, S., 2020. Field phenotyping of plant height in an upland rice field in Laos using low-cost small unmanned aerial vehicles (UAVs). *Plant Prod. Sci.* 00, 1–14. <https://doi.org/10.1080/1343943X.2020.1766362>.
- Kendall, S.L., Holmes, H., White, C.A., Clarke, S.M., Berry, P.M., 2017. Quantifying lodging-induced yield losses in oilseed rape. *F. Crop. Res.* <https://doi.org/10.1016/j.fcr.2017.06.013>.
- Liu, T., Li, R., Zhong, X., Jiang, M., Jin, X., Zhou, P., Liu, S., Sun, C., Guo, W., 2018. Estimates of rice lodging using indices derived from UAV visible and thermal infrared images. *Agric. For. Meteorol.* <https://doi.org/10.1016/j.agrformet.2018.01.021>.
- Maimaitijiang, M., Sagan, V., Sidiqe, P., Daloye, A.M., Erkbol, H., Fritsch, F.B., 2020. Crop monitoring using satellite/UAV data fusion and machine learning. *Remote Sens.* 12 <https://doi.org/10.3390/RS12091357>.
- Mardanisamani, S., Maleki, F., Kassani, S.H., Rajapaksa, S., Duddu, H., Wang, M., Shirtliffe, S., Ryu, S., Josutties, A., Zhang, T., Vail, S., Pozniak, C., Parkin, I., Stavness, I., Eramian, M., 2019. Crop Lodging Prediction from UAV-Acquired Images of Wheat and Canola using a DCNN Augmented with Handcrafted Texture Features.
- Masuda, R., Fujimoto, S., Iida, M., Suguri, M., 2013. A method to detect the occurrence of rice plant lodging using wavelet transform. In: IFAC Proceedings Volumes (IFAC-PapersOnline). IFAC. <https://doi.org/10.3182/20130828-2-SF-3019.00048>.
- Mortensen, A.K., Laursen, M.S., Jørgensen, R.N., Gislum, R., 2019. Drone dataflow - a MATLAB toolbox for extracting plots from images captured by a UAV. In: Proc. 12th Eur. Conf. Precis. Agric, pp. 959–965.
- Murakami, T., Yui, M., Amaha, K., 2012. Canopy height measurement by photogrammetric analysis of aerial images: Application to buckwheat (*Fagopyrum esculentum* Moench) lodging evaluation. *Comput. Electron. Agric.* <https://doi.org/10.1016/j.compag.2012.08.003>.
- Niu, L., Feng, S., Ru, Z., Li, G., Zhang, Z., Wang, Z., 2012. Rapid determination of single-stalk and population lodging resistance strengths and an assessment of the stem lodging wind speeds for winter wheat. *F. Crop. Res.* <https://doi.org/10.1016/j.fcr.2012.10.014>.
- Ogden, R.T., Miller, C.E., Takezawa, K., Ninomiya, S., 2002. Functional regression in crop lodging assessment with digital images. *J. Agric. Biol. Environ. Stat.* <https://doi.org/10.1198/108571102339>.
- Orynbaykzy, A., Gessner, U., Conrad, C., 2019. Crop type classification using a combination of optical and radar remote sensing data: a review. *Int. J. Remote Sens.* 40, 6553–6595. <https://doi.org/10.1080/01431161.2019.1569791>.
- Poley, L.G., McDermid, G.J., 2020. A systematic review of the factors influencing the estimation of vegetation aboveground biomass using unmanned aerial systems. *Remote Sens.* 12 <https://doi.org/10.3390/rs12071052>.
- Rajapaksa, S., Eramian, M., Duddu, H., Wang, M., Shirtliffe, S., Ryu, S., Josutties, A., Zhang, T., Vail, S., Pozniak, C., Parkin, I., 2018. Classification of crop lodging with gray level co-occurrence matrix. In: Proceedings - 2018 IEEE Winter Conference on Applications of Computer Vision, WACV 2018. <https://doi.org/10.1109/WACV.2018.00034>.
- Skovsen, S., Dyrmann, M., Mortensen, A.K., Steen, K.A., Green, O., Eriksen, J., Gislum, R., Jørgensen, R.N., Karstoft, H., 2017. Estimation of the botanical composition of clover-grass leys from RGB images using data simulation and fully convolutional neural networks. *Sensors (Switzerland)* 17. <https://doi.org/10.3390/s17122930>.
- Skovsen, S.K., Laursen, M.S., Kristensen, R.K., Rasmussen, J., Dyrmann, M., Eriksen, J., Gislum, R., Jørgensen, R.N., Karstoft, H., 2021. Robust species distribution mapping of crop mixtures using color images and convolutional neural networks. *Sensors* 21, 1–28.
- Tan, M., Le, Q.V., 2019. EfficientNet: Rethinking Model Scaling for Convolutional Neural Networks arXiv.
- Teimouri, N., Dyrmann, M., Jørgensen, R.N., 2019. A novel spatio-temporal FCN-LSTM network for recognizing various crop types using multi-temporal radar images. *Remote Sens.* 11, 990. <https://doi.org/10.3390/rs11080990>.
- Wang, J.J., Ge, H., Dai, Qigen, Ahmad, I., Dai, Qixing, Zhou, G., Qin, M., Gu, C., 2018. Unsupervised discrimination between lodged and non-lodged winter wheat: a case study using a low-cost unmanned aerial vehicle. *Int. J. Remote Sens.* <https://doi.org/10.1080/01431161.2017.1422875>.
- Wilke, N., Siegmann, B., Klingbeil, L., Burkart, A., Kraska, T., Muller, O., van Doorn, A., Heinemann, S., Rascher, U., 2019. Quantifying lodging percentage and lodging severity using a UAV-based canopy height model combined with an objective threshold approach. *Remote Sens.* <https://doi.org/10.3390/rs11050515>.
- Xue, J., Xie, R.zhi, Zhang, W.feng, Wang, K.Ru, Hou, P., Ming, B., Gou, L., Li, S., 2017. Research progress on reduced lodging of high-yield and -density maize. *J. Integr. Agric.* [https://doi.org/10.1016/S2095-3119\(17\)61785-4](https://doi.org/10.1016/S2095-3119(17)61785-4).

- Yang, M.Der, Huang, K.S., Kuo, Y.H., Tsai, H.P., Lin, L.M., 2017. Spatial and spectral hybrid image classification for rice lodging assessment through UAV imagery. *Remote Sens.* <https://doi.org/10.3390/rs9060583>.
- Yang, H., Chen, E., Li, Z., Zhao, C., Yang, G., Pignatti, S., Casa, R., Zhao, L., 2015. Wheat lodging monitoring using polarimetric index from RADARSAT-2 data. *Int. J. Appl. Earth Obs. Geoinf.* <https://doi.org/10.1016/j.jag.2014.08.010>.
- Zhang, J.C., Gu, X.H., Wang, J.H., Huang, W.J., Dong, Y.Y., Luo, J.H., Yuan, L., Li, Y.F., 2012. Evaluating maize grain quality by continuous wavelet analysis under normal and lodging circumstances. *Sens. Lett.* <https://doi.org/10.1166/sl.2012.1871>.